PNAS RESEARCH ARTICLE | PLANT BIOLOGY

Single-molecule views of chromatin accessibility and structure during photomorphogenesis

Lei Li[a,b,1], Guanyu Chen[a,b,1], Guangquan Zhu[a], Jili Wu[a], Xinglong Kui[a], Zihui Zhang[b], Lingyang Feng[b], Minghan Huang[b,c], Wenbo Hua[d], Zhipeng Qu[e], Lina Zou[e], Changmei Lu[a], Bojian Zhong[a], Hang He[b,c], Xing Wang Deng[b,c,2], and Linhua Sun[a,b,2]

Affiliations are included on p. 12.

Contributed by Xing Wang Deng; received June 26, 2025; accepted November 3, 2025; reviewed by Roger B. Deal, Alexandre P. Marand, Robert J. Schmitz, and Jixian Zhai

The dynamic organization of chromatin governs gene expression by regulating DNA accessibility. In plants, light not only initiates photomorphogenesis but also reshapes higher-order chromatin architecture. However, the limited resolution of current techniques impedes investigation of chromatin dynamics at the single-molecule level. Here, we applied Fiber-seq, a long-read, single-molecule chromatin profiling method, to construct near-nucleotide resolution maps of chromatin accessibility, nucleosome positioning, and cytosine methylation in *Arabidopsis thaliana* and maize. We observed that light exposure during photomorphogenesis led to significant, locus-specific changes in chromatin accessibility—both increases and decreases—especially in genes related to photosynthesis, hormone signaling, and development. Analysis of chromatin accessibility changes in *cop1-6*, *pifq*, and *hy5 hyh* mutants revealed that classical light signaling pathways regulate chromatin accessibility. Additionally, using high-fidelity long-read sequencing, we profiled DNA methylation in previously inaccessible repetitive regions such as 5S rRNA gene clusters and *CEN180* satellite repeats. These heterochromatic loci exhibited distinct light-dependent changes in chromatin accessibility that were undetectable using prior methods. In maize, we demonstrated that Fiber-seq identifies a broader range of biologically relevant open chromatin regions, enabling both high-accuracy de novo genome assembly and the detection of fine-scale structural variants. Collectively, Fiber-seq offers an integrated view of chromatin states across regulatory and repetitive elements, providing critical insights into how environmental signals reshape plant epigenomes.

fiber-seq | photomorphogenesis | chromatin accessibility | genome variation

Significance

Environmental cues, such as light, profoundly influence plant development; however, the chromatin-level mechanisms underlying these responses remain poorly understood due to technical limitations. Here, we applied Fiber-seq, a long-read, single-molecule chromatin profiling method, to simultaneously map chromatin accessibility, nucleosome positioning, and cytosine methylation in *Arabidopsis* and maize. This approach reveals previously undetectable, light-induced changes in both regulatory and heterochromatic regions, including gene clusters and centromeric repeats. By integrating chromatin architecture with de novo genome assembly and structural variation analysis, Fiber-seq provides a robust framework for decoding how environmental signals dynamically reprogram plant epigenomes at high resolution.

Light is one of the most critical environmental factors for plant growth and development; it serves not only as an energy source but also as an important signal, playing a pivotal role throughout the plant's life cycle (1). Plants have evolved complex and sophisticated transcriptional networks to mediate developmental changes in response to light. These light-regulated processes include seedling photomorphogenesis, seed germination, shade avoidance, and photoperiod responses (2). The light signal transduction pathway perceives changes in different light qualities (far-red, red, and blue light) through various photoreceptors, such as phytochromes and cryptochromes, subsequently triggering extensive reprogramming of downstream gene expression (3, 4). During photomorphogenesis, CONSTITUTIVE PHOTOMORPHOGENIC 1 (COP1) is a key regulator. In darkness, the E3 ubiquitin ligase COP1 promotes the proteasome-mediated degradation of positive regulators such as ELONGATED HYPOCOTYL 5 (HY5), HY5 HOMOLOG (HYH), LONG AFTER FAR-RED LIGHT 1 (LAF1), LONG HYPOCOTYL IN FAR-RED 1 (HFR1), thereby suppressing light-responsive gene expression under dark conditions. Upon exposure to light, COP1 is excluded from the nucleus, allowing these transcription factors (TFs) to accumulate and initiate the photomorphogenic program (5). Concurrently, TFs directly interact with genes to regulate transcription. For example, the bHLH proteins PHYTOCHROME-INTERACTING FACTORs (PIFs) and the plant-specific proteins ETHYLENE-INSENSITIVE 3/EIN3-LIKE 1 (EIN3/EIL1) accumulate in darkness to maintain skotomorphogenesis. In contrast, the bZIP proteins HY5 and HYH are stabilized in light and promote photomorphogenic development (6). HY5, as a key TF, functions downstream of multiple photoreceptors, and mutations in its gene lead to various photomorphogenesis defects (7). Research concerning light-responsive elements (LREs) has further demonstrated that combinations of these elements, rather than individual elements alone, can facilitate the plant's ability to coordinate light signals with its developmental stage to regulate

Reviewers: R.B.D., Emory University; A.P.M., University of Michigan; R.J.S., University of Georgia; and J.Z., Southern University of Science and Technology Department of Biology.

The authors declare no competing interest.

[1]L.L. and G.C. contributed equally to this work.

[2]To whom correspondence may be addressed. Email: deng@pku.edu.cn or sunlh@njnu.edu.cn.

This article contains supporting information online at https://www.pnas.org/lookup/suppl/doi:10.1073/pnas.2516708122/-/DCSupplemental.

Published November 26, 2025.

gene expression. Furthermore, their activity can be modulated by the phytochrome system (8).

Plants precisely respond to light signals by dynamically regulating epigenetic states, thereby achieving more persistent control over gene expression. Studies have revealed that light regulates histone modifications through photoreceptors and key light-signaling proteins [such as DE-ETIOLATED 1 (DET1)]—including H3K4me3, H3K9ac, H3K9me2, H3K27me3, and histone H2B monoubiquitination (H2Bub)—thereby influencing the expression of light-responsive genes (9–11). Simultaneously, light also regulates deacetylation; for example, HISTONE DEACETYLASE 19 (HDA19) forms a complex with PIF1/PIF3 and Mediator subunit 25 (MED25), inhibiting phytochrome signaling pathways through histone deacetylation (12). Furthermore, light can affect chromatin remodeling and nucleosome density. For instance, PHYTOCHROME B (PHYB) and HISTONE DEACETYLASE 6 (HDA6) cooperatively regulate light-induced chromatin compaction (13). *Arabidopsis* cryptochrome 1 (CRY1) controls photomorphogenesis by regulating H2A.Z histone variant deposition (14). Additionally, the transcriptional regulator PIF7 and the histone H3K27-demethylase RELATIVE OF EARLY FLOWERING 6 (REF6) play crucial roles in plant shade avoidance memory, where PIF7 accumulation induces REF6 recruitment to demethylate H3K27me3 on the chromatin of relevant genes (15). COP1 interacts with the Polycomb protein VIN3-LIKE 1 (VIL1), governs light-dependent chromatin loop formation, and limits a repressive histone modification to fine-tune photomorphogenesis and gene expression (16, 17). These findings collectively reveal pathways for transcriptional regulation through light-mediated epigenetic mechanisms, providing key insights into how plants dynamically respond to environmental signals via chromatin remodeling.

However, whether and to what extent light modulates chromatin accessibility, and how such changes are integrated with classical light signaling pathways, remains poorly understood. A previous study employed DNase I hypersensitive site sequencing (DNase-seq) to generate a genome-wide map of chromatin accessibility in *Arabidopsis* under various light conditions, revealing widespread DNase I hypersensitive sites and TF footprints (18). The mechanistic connection between light-driven chromatin remodeling and key regulators such as COP1, HY5, and PIFs remains incompletely understood. Specifically, the precise role of light in orchestrating these dynamic chromatin changes has yet to be fully elucidated.

Chromatin accessibility profiling methods based on second-generation sequencing, such as DNase-seq and assay for transposase-accessible chromatin using sequencing (ATAC-seq), are limited in complex plant genomes due to high repeat content and structural complexity. For instance, maize has 88.37% repetitive sequences (19), and even *Arabidopsis* contains complex rRNA clusters (20). These methods cannot fully resolve chromatin structure or single-molecule accessibility. In contrast, third-generation sequencing, particularly Pacific Biosciences of California (PacBio) HiFi sequencing, offers approximately 99.8% accuracy (Q30) and long-read capability (21), enabling precise base modification detection (22) and telomere-to-telomere (T2T) assembly in complex genomic regions (23). Building on these advantages, several long-read sequencing-based methods—such as single-molecule chromatin fiber sequencing (Fiber-seq) (24), single-molecule adenine-methylated oligonucleosome sequencing assay by tagmentation (SAMOSA-Tag) (25), single-molecule targeted accessibility and methylation sequencing (STAM-seq) (26), and single-molecule accessibility and methylation sequencing (SAM-seq) (27)—have recently been developed to profile chromatin accessibility at single-molecule resolution, offering new opportunities to investigate chromatin dynamics in response to environmental cues like light.

In this study, we applied Fiber-seq, which integrates adenine methyltransferase labeling (Hia5) (24) with PacBio HiFi sequencing, to achieve near-nucleotide resolution profiling of chromatin accessibility, nucleosome organization, and CG methylation (mCG) in plants. In *Arabidopsis*, we captured dynamic chromatin changes specifically driven by light during photomorphogenesis, revealing how these external light cues and endogenous signaling pathways collectively shape the epigenome, including within repetitive regions. In maize, a joint analysis of chromatin accessibility and structural variation (SV) based on de novo genome assembly demonstrated the advantage of Fiber-seq in detecting open chromatin regions. These results underscore the utility of Fiber-seq for dissecting plant chromatin architecture and provide a foundation for future studies in environmental adaptation and breeding.

Results

m6A Stencils Reveal Single-Molecule Chromatin Accessibility in *Arabidopsis*. We used N^6-adenine DNA methyltransferase (m6A-MTase) to label accessible adenine sites, using the Hia5 enzyme to mark these open regions (*SI Appendix*, *Materials and Methods* and Fig. S1). Single-molecule accessibility information was then obtained via third-generation sequencing. Based on long and continuous clusters of labeled m6A, we identified open chromatin and linker DNA, from which nucleosome positioning signals were subsequently inferred (Fig. 1*A*). We tested two library preparation methods that accommodate different starting sample quantities and employ distinct fragment selection approaches. For replicate 1, we constructed a 10-kb HiFi library using AMPure PB beads. For replicate 2, a 15-kb HiFi library was constructed using the Pippin HT system. We performed quality control on the resulting HiFi sequences; replicate 1 had an average molecular length of 14,219 bp, and replicate 2 averaged 19,932 bp. Both replicates showed high Q-values, indicating excellent sequence quality from both methods (Fig. 1*B* and Dataset S1). In the absence of methyltransferase treatment, m6A modification is almost undetectable on DNA. However, on the *PHOTOSYSTEM II LIGHT HARVESTING COMPLEX GENE 2.1* (*LHCB2.1*) promoter, we observed clustered m6A in chromatin open regions after treatment with the methyltransferase. By generating a large number of reads through HiFi sequencing, each carrying m6A modification information, we quantified the number of m6A signals at each site and used Fibertools (28) to remove background noise. Regions with consecutive m6A marks are defined as Fiber-seq inferred regulatory elements (FIREs), which showed consistent positioning with open chromatin regions identified by both ATAC-seq (29) and DNase-seq (30) (Fig. 1*C*). Fiber-seq can also detect linker DNA, nucleosomes, and mCG positions. We observed the local chromatin state on the longer gene, such as the *HOLOCARBOXYLASE SYNTHASE 1* (*HCS1*) gene, and found that most fibers are open in the promoter region. Outside these open regions, nucleosomes exhibited a periodic oscillation pattern, with linker DNA positions complementary to nucleosome positions (Fig. 1*D*). We observed a greater variety of chromatin accessibility patterns in other genes. For instance, *SUPPRESSOR OF drm1 drm2 cmt3* (*SDC*) is not accessible, but its promoter region exhibits high levels of CG methylation (31). In contrast, the promoter of a nearby gene is accessible but lacks CG methylation. The promoter of *YUCCA8* (*YUC8*) is accessible (*SI Appendix*, Fig. S2). *ARABIDOPSIS THALIANA HOMEOBOX-LEUCINE*

ZIPPER PROTEIN 4 (*ATHB4*) contains multiple open regions, while *CASEIN KINASE 1-LIKE PROTEIN 3* (*CKL3*) has an open promoter, with mCG present in the nonopen areas (*SI Appendix*, Fig. S3). Despite the differences in size selection methods, the correlation between the two *Arabidopsis* biological replicates remained high, confirming the high reproducibility of Fiber-seq (Fig. 1*E*). We then compared peaks detected by Fiber-seq and ATAC-seq (29), finding that overlap peaks account for 74.3% of ATAC-seq peaks and 79.2% of Fiber-seq peaks (*P*-value calculated by a permutation test) (Fig. 1*F* and Dataset S2). Meta gene analysis revealed that Fiber-seq and ATAC-seq exhibit highly similar peak profiles, characterized by strong chromatin accessibility and reduced nucleosome occupancy at transcription start sites (TSSs) (Fig. 1*G* and *SI Appendix*, Fig. S4).

Taken together, these results indicate that Fiber-seq not only maps chromatin accessibility at single-molecule resolution but also accurately determines nucleosome positioning and DNA methylation patterns at high resolution. This technique enables simultaneous analysis of these structural and functional features, providing insights into the fundamental principles of chromatin organization in plants.

Patterns of Nucleosome Positioning and Chromatin Accessibility. To illustrate the periodic oscillation of nucleosome signals and its relationship with gene expression in detail, we started our observations at the TSS. From the TSS, we could clearly see nucleosome levels decrease in open regions, followed by a distinct periodic oscillation pattern, which is consistent with published MNase-seq data (32–34) (*SI Appendix*, Fig. S5 *A–H*). The linker DNA signals consistently remained complementary to the nucleosome signals (Fig. 2*A* and *SI Appendix*, Fig. S5*I*). We then categorized all *Arabidopsis* protein-coding genes into nine groups based on their expression levels, from the lowest to the highest, with roughly equal numbers of genes per group. We found that genes with higher expression levels also exhibited greater chromatin accessibility at the TSS (Fig. 2*B* and *SI Appendix*, Fig. S5*J*). At TSS, higher gene expression levels are associated with lower nucleosome occupancy and more pronounced nucleosome periodicity downstream (Fig. 2*C* and *SI Appendix*, Fig. S5*K*). This suggests a potential relationship between chromatin accessibility, nucleosomes, and gene expression. To better observe nucleosome organization, we aligned signals starting from the +1 nucleosome and examined the distribution patterns of FIREs, nucleosomes, and linker DNA. This alignment further clarified nucleosome positioning and its complementary relationship with linker DNA (Fig. 2*D* and *SI Appendix*, Fig. S5*L*). When genes were sorted by Fiber-seq score from high to low, the periodicity of nucleosomes became apparent. In downstream open regions, we observed the ordered arrangement of 5 to 6 nucleosomes. Linker DNA are also clearly visible, shorter, and complementary to the nucleosome signals (Fig. 2*E*).

Furthermore, owing to Fiber-seq's near-nucleotide resolution, we were able to resolve TF binding motifs with high specificity. We indeed identified footprints in the binding regions of transcriptional factors (35), including EIN3, PIF1, PIF4, and PSEUDO-RESPONSE REGULATOR 5 (PRR5), which were visualized as abrupt drops in raw m6A methylation rates (*SI Appendix*, Fig. S6 *A–D*). To further investigate the pattern of long-range regulatory elements, we collected potential enhancers from prior studies (30, 36). In these enhancer regions, chromatin is in an open state, characterized by low nucleosome signals, indicating that Fiber-seq can also be used to predict enhancers, similar to ATAC-seq and DNase-seq (*SI Appendix*, Fig. S6 *E* and *F*). Cohesin plays a crucial role in maintaining chromosome structure and regulating transcription. Cohesin is a ring structure composed of SISTER CHROMATID ADHESION 3 (SCC3), STRUCTURE MAINTENANCE OF CHROMOSOME (SMC1) and SMC3, and α-kleisin family proteins. The α-kleisin is composed of SISTER CHROMATID COHESION 1 PROTEIN 1-4 (SYN1-4), among which SYN4 interacts with SCC3 (37). We used SCC3 and SYN4 ChIP-seq binding sites to indicate cohesin binding sites (37). The high accessibility and low nucleosome signal at these binding sites show that cohesin binding sites are open (*SI Appendix*, Fig. S6 *G* and *H*). To further unravel the relationship between enhancers, cohesin, and chromatin organization, we used high-throughput chromosome conformation capture (Hi-C) (38) and Micro-C-XL (39) to observe interactions among *cis*-regulatory elements. We identified some potential enhancers of *ARABIDOPSIS THALIANA HOMEOBOX PROTEIN 2* (*ATHB2*) that exhibit complex chromatin interactions. These enhancers contain multiple G-box (CACGTG) elements and show both ATAC-seq and DNase-seq signals. Based on Fiber-seq results, we observed that the accessibility of these enhancers may be coregulated at the single-molecule level. Furthermore, they display strong cohesin and PIFs binding (*SI Appendix*, Fig. S6*I*). Similar enhancer interaction patterns were observed at the *TEOSINTE BRANCHED, cycloidea and PCF 14* (*TCP14*), *ARABIDOPSIS THALIANA HOMEOBOX PROTEIN 6* (*ATHB-6*) loci (*SI Appendix*, Figs. S6*J* and S7).

These results collectively demonstrate that *Arabidopsis* gene regulation operates through a tightly coordinated system, where chromatin accessibility at enhancers, cohesin-mediated chromatin looping, and TF binding converge to influence changes in gene expression levels.

Dynamic Chromatin Accessibility During Photomorphogenesis. To investigate the effect of light on chromatin accessibility, we designed a dark-to-light transition experiment with five conditions: 5 d of complete darkness (D), 1 h of light after darkness (D1L), 6 h of light after darkness (D6L), 24 h of light after darkness (D24L), and 5 d of continuous light (L). With increasing light exposure, *Arabidopsis* exhibits phenotypic changes, including hypocotyl shortening, cotyledon opening, and greening. We performed Fiber-seq and RNA-seq within this system, using Fiber-seq to identify open chromatin regions, nucleosomes, and mCG signals (Fig. 3*A* and *Materials and Methods*). During the photomorphogenesis process, we identified photodynamic peaks, specifically 3,665 FIRE variable peaks, 2,118 nucleosome variable peaks, and 595 differentially methylated regions (DMRs) (Fig. 3*B* and Datasets S3 and S4 and *SI Appendix*, Fig. S8*A*). To illustrate the dynamic changes occurring during this process, we performed principal component analysis (PCA) on data from all three omics types. The results demonstrated excellent sample reproducibility, and the changes in FIREs and nucleosomes during photomorphogenesis exhibited a certain regularity (Fig. 3*B*). We further investigated the relationship between these photodynamic peaks and gene expression and found that approximately 16.3% of the photodynamic peaks were associated with genes that also exhibited changes in expression levels (Fig. 3*C*).

Based on photodynamic changes in chromatin accessibility during the light transition, genes associated with variable accessibility were grouped into eight distinct clusters using K-means clustering, with the clusters arranged according to their temporal patterns. Each cluster exhibits distinct patterns of accessibility changes, reflecting differential chromatin responses to light regulation. To further elucidate the biological relevance of these clusters, we identified and annotated typical genes that exhibit accessibility changes within each cluster. Among them, genes such as *PHOTOSYSTEM II LIGHT HARVESTING COMPLEX*

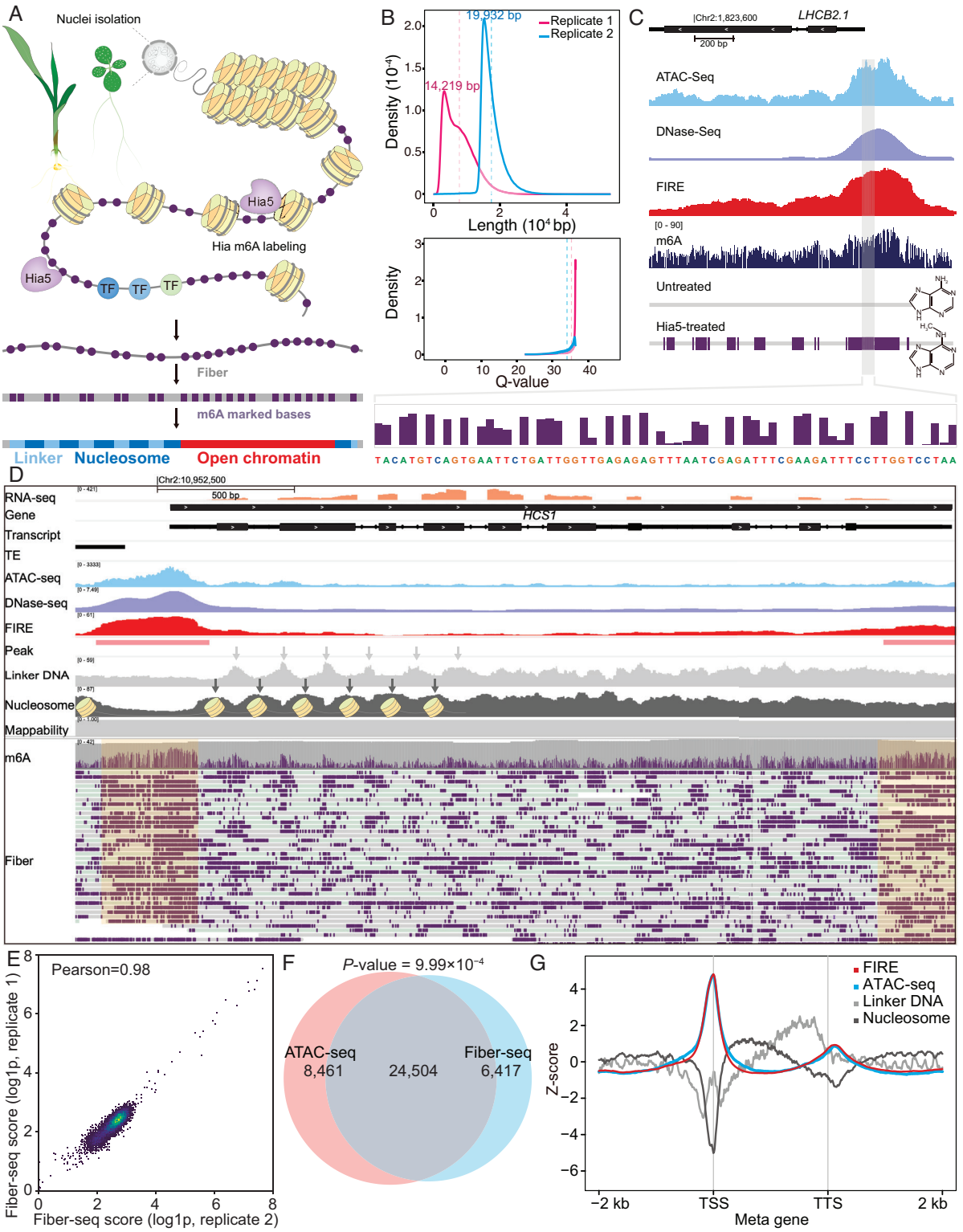

Fig. 1. Probe open chromatin and DNA methylation in *Arabidopsis* by Fiber-seq. (*A*) Experimental schematic of Fiber-seq. Nuclei were isolated and treated with N^6-methyladenine methyltransferase (m6A-MTase) to label accessible chromatin regions. Long-read sequencing was used to identify methylated adenine sites, which were then used to infer open chromatin regions, nucleosome positions, and linker DNA. Chromatin fibers are shown in gray, methylated adenines are represented as purple dots, predicted linker DNA regions are in light blue, nucleosomes are in dark blue, and the open chromatin identified based on FIREs is in red. (*B*) Histogram showing the distribution of chromatin fiber lengths obtained from *Arabidopsis* Fiber-seq, including average read length and Q-value. (*C*) Comparative analysis of ATAC-seq, DNase-seq, and Fiber-seq at the *PHOTOSYSTEM II LIGHT HARVESTING COMPLEX GENE 2.1* (*LHCB2.1*) locus. Tracks include ATAC-seq signal, DNase-seq signal, FIREs, m6A levels, and an illustration of m6A-marked sites on chromatin fibers before and after Hia5 treatment. Chromatin fibers are shown in gray, and short vertical purple lines mark m6A sites. (*D*) Comparative profiling at the *HOLOCARBOXYLASE SYNTHASE 1 (HCS1)* locus, showing RNA-seq, ATAC-seq, DNase-seq, FIREs, peaks, linker DNA, nucleosome positions, mappability, total adenine methylation, and per-fiber methylation. Chromatin fibers are shown in gray, with m6A sites represented as short purple lines. Arrows indicate the location of the linker DNA and nucleosome, and yellow highlights indicate accessible chromatin regions. (*E*) Reproducibility between two *Arabidopsis* Fiber-seq samples. Pearson's correlation coefficient was used to evaluate the similarity of identified open chromatin regions between two biological replicates. The Fiber-seq score indicates the absolute value of m6A at the same site after background subtraction. (*F*) Overlap analysis between ATAC-seq and Fiber-seq peaks, with *P*-value calculated using a permutation test. (*G*) Meta gene analysis of the distribution of FIREs, ATAC-seq, linker DNA, and nucleosomes at TSSs and transcription termination sites (TTSs) in *Arabidopsis*.

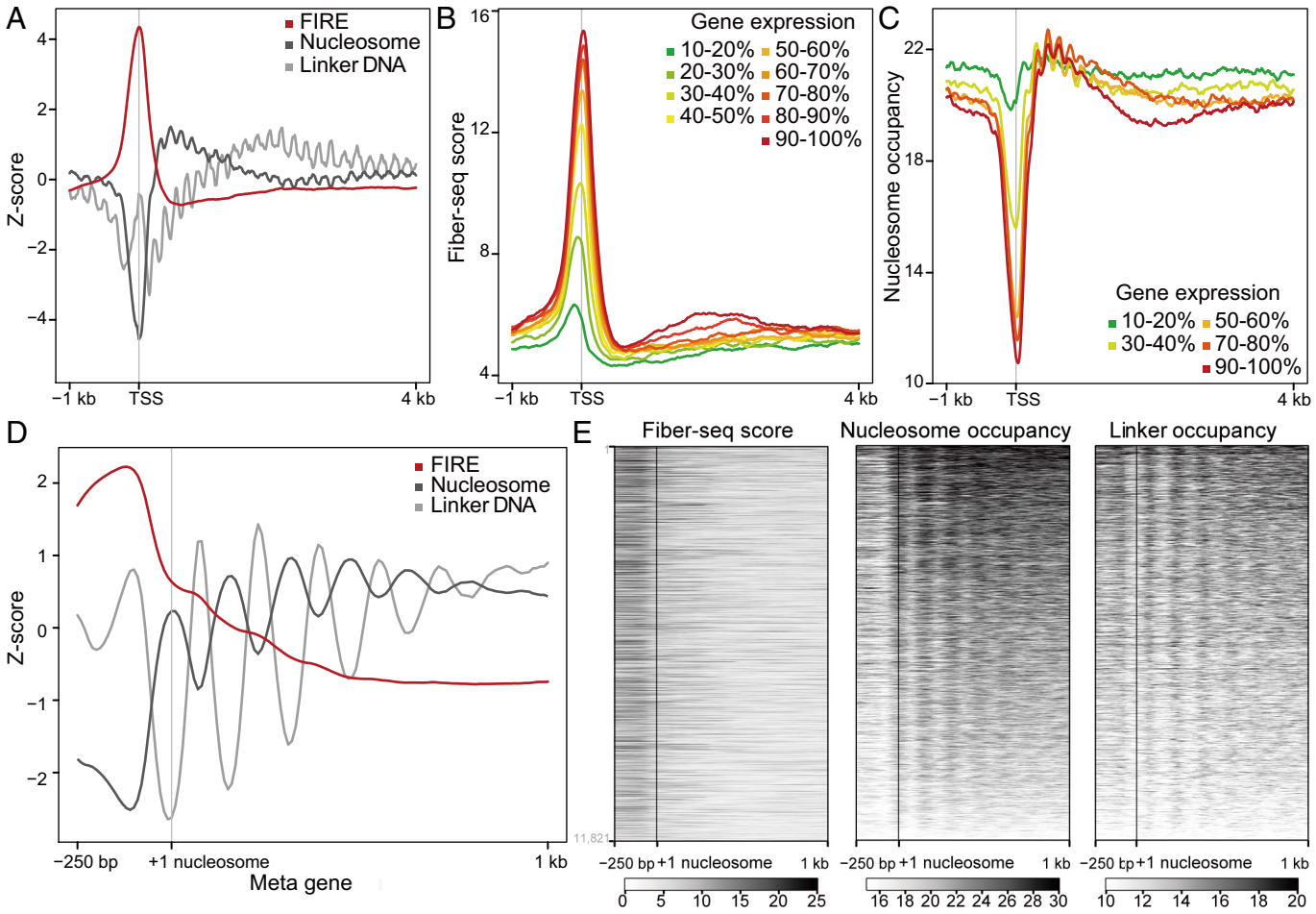

Fig. 2. Nucleosome occupancy in *Arabidopsis*. (*A*) Meta gene analysis of FIRE, linker DNA, and nucleosomes at TSS. (*B* and *C*) Peak changes in Fiber-seq signals and nucleosome occupancy across various gene expression levels. Nine groups were divided according to gene expression levels for comparative analysis. (*D*) Meta gene analysis of FIRE, linker DNA, and nucleosomes at the +1 nucleosome position. The randomized control plots for (*A–D*) are shown in *SI Appendix*, Fig. S5 *I–L*. (*E*) Heatmap showing the distribution of FIRE, linker DNA, and nucleosomes starting from the +1 nucleosome.

GENE 2.3 (*LHCB2.3*), *ROOT PHOTOTROPISM 2* (*RPT2*), *ATHB4*, and *LONG HYPOCOTYL IN FAR-RED* (*HFR1*) are central to how plants perceive light and adjust their development accordingly (40) (Fig. 3*D* and Dataset S5). To further investigate the functional specificity of each cluster, we performed Gene Ontology (GO) analysis of the peak-associated genes. Cluster 8 showed significant enrichment in light signal transduction, hormone responses, and gene expression regulation. Meanwhile, Cluster 3 was significantly enriched in transcription, metabolism, and system development (Fig. 3*E* and Dataset S6).

To gain further insight into the regulatory features of each cluster, we examined the genomic distribution of accessibility peaks. Across all clusters, peaks were most densely located in promoter regions, followed by intergenic and exon regions, indicating a predominant regulatory role at the TSS (*SI Appendix*, Fig. S8*B*). Interestingly, cluster 5 exhibited the highest proportion of promoter-associated peaks and the lowest proportion in exons. In contrast, cluster 7 showed the opposite trend, with fewer promoter-associated peaks and a higher proportion of peaks within exons. These contrasting patterns suggest potential functional differences in the regulatory roles of these clusters (*SI Appendix*, Fig. S8*B*). Furthermore, we examined the distribution of peaks associated with genes and transposable elements (TEs). We observed that most peaks were located in gene regions, suggesting a role in gene regulation. A smaller proportion, approximately 15%, was found in TE regions, indicating that TEs also possess potential regulation (*SI Appendix*, Fig. S8*C*).

Additionally, we investigated FIRE dynamics and fiber-level chromatin accessibility at representative gene loci. *HFR1* (41), a key regulator of de-etiolation, is predominantly active during early light responses but exhibited reduced activity under continuous light, which is reflected in its low chromatin accessibility under constant light conditions. Conversely, *LHCB2.3* (42), which encodes a Photosystem II protein involved in light energy capture during photosynthesis, showed a gradual increase in chromatin accessibility under illuminated conditions, suggesting its light-induced activation (Fig. 3*F*). We further investigated chromatin accessibility changes at several other light-responsive gene loci. Both *RPT2* (43), involved in phototropic responses, and *ATHB4* (44), which participates in shade avoidance, exhibited their lowest chromatin accessibility after 6 h of light exposure. This suggests a transient repression or regulatory shift during the early phase of the light response. *ATHB2* (45) is a homeodomain-leucine zipper TF and is induced by shade and low red/far-red light. The multiple open chromatin regions before the TSS of this gene show complex dynamic changes. In addition, *LIGHT-HARVESTING CHLOROPHYLL A/B-BINDING PROTEIN 2* (*LHCA2*) (46) is a core component of Photosystem I responsible for capturing and transferring light energy. Its accessibility may be directly proportional to the duration of light exposure (*SI Appendix*, Fig. S9).

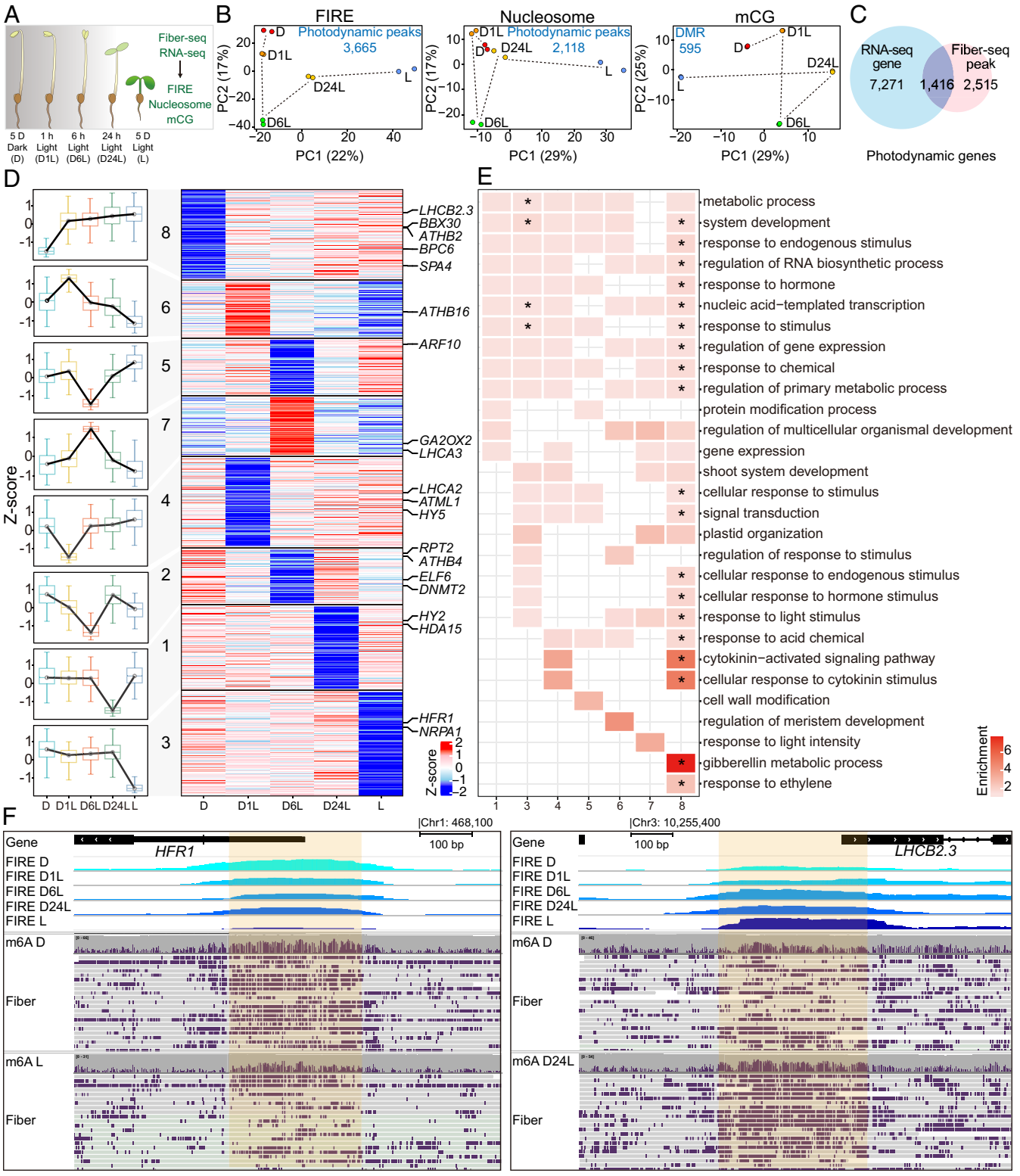

Fig. 3. Chromatin accessibility dynamics during photomorphogenesis in *Arabidopsis*. (*A*) Schematic illustration of phenotypic changes in wild-type (WT) *Arabidopsis* during light transition, along with key technologies. (*B*) PCA of FIRE, nucleosome positioning, and CG methylation (mCG) across the five sample groups during the light transition. Photodynamic peaks refer to the union of differentially accessible peaks obtained from all pairwise comparisons among the five *Arabidopsis* samples used in our study: 5-d dark treatment (D), 1-h light treatment (D1L), 6-h light treatment (D6L), 24-h light treatment (D24L), and 5-d light treatment (L). (*C*) During photomorphogenesis, the relationship between the number of genes with transcriptional changes and the number of genes corresponding to peaks showing altered chromatin accessibility in WT *Arabidopsis*. Photodynamic genes refer to the union of differentially expressed genes obtained from all pairwise comparisons among the five *Arabidopsis* samples used in our study: D, D1L, D6L, D24L, and L. (*D*) Heatmap showing genes corresponding to peaks with altered accessibility during the light transition, grouped into eight clusters based on accessibility patterns. The characteristic accessibility trends of the eight clusters are further visualized using box plots, with key genes labeled. (*E*) Gene ontology (GO) pathways and their enrichment across the eight accessibility clusters for genes associated with peaks. The box colors indicate the enrichment score of each GO term. The enrichment score is computed as (Number of input genes in a GO term/Total input genes) divided by (Number of genes in the GO term/Total genes). An asterisk (*) indicates false discovery rate (FDR) < 0.05. (*F*) FIRE signals at the *LONG HYPOCOTYL IN FAR-RED* (*HFR1*) and *PHOTOSYSTEM II LIGHT HARVESTING COMPLEX GENE 2.3* (*LHCB2.3*) loci during the light transition. Fiber views at the *HFR1* locus are shown for the D and L samples, while the *LHCB2.3* locus includes fiber data for D and D24L samples. Yellow highlights indicate regions with notable peak changes.

These results collectively demonstrate that light dynamically and specifically regulates chromatin accessibility during photomorphogenesis, highlighting a tightly coordinated chromatin reprogramming process that extends beyond simple switches.

Classical Light Signaling Pathways Regulate Chromatin Accessibility. To investigate whether changes in chromatin accessibility depend on classical light signaling pathways, we performed Fiber-seq and RNA-seq under the following conditions: *cop1-6* (D), *cop1-6* (L), *pifq* (*pif1 pif3 pif4 pif5*) (D), *hy5 hyh* (D), and *hy5 hyh* (L). We performed PCA on the transcriptomes of all samples, and the results showed good reproducibility for each sample (Fig. 4*A* and Dataset S7). Excellent reproducibility was also observed in their FIRE and nucleosome PCA analyses (*SI Appendix*, Fig. S10 *A* and *B*). The relationship between chromatin accessibility and gene expression in mutants was analyzed in comparison to the wild type under specific conditions. The results showed that the proportion of accessibility changes accompanied by expression changes was 21.0% in *cop1-6* (D), 6.4% in *cop1-6* (L), 21.5% in *pifq* (D), 3.2% in *hy5 hyh* (D), and 3.2% in *hy5 hyh* (L) (Dataset S8 and *SI Appendix*, Fig. S10*C*). This could be due to the complexity of gene regulatory mechanisms, with certain open chromatin regions controlling the expression of distant genes.

To explore whether light-induced changes in chromatin states depend on canonical light signaling pathways, we conducted a heatmap analysis of chromatin accessibility in WT (D), WT (L), *cop1-6* (D), *pifq* (D), and *hy5 hyh* (L). Focusing on clusters defined by regions where accessibility changes in WT during the dark-to-light transition, *cop1-6* and *pifq* mutants exhibit light-like chromatin accessibility states when grown in darkness (Fig. 4*B*). Specifically, in cluster 8, the accessibility of dark-grown *cop1-6* is relatively high, resembling that under light. In contrast, in cluster 3, the accessibility of dark-grown *cop1-6* is relatively low, also resembling that under light. Concurrently, we observed a phenomenon similar to *cop1-6* in *pifq* mutants. And in clusters 3 and 8, the accessibility of *hy5 hyh* was relatively higher compared to that under light conditions (Fig. 4*C* and *SI Appendix*, Fig. S10*D*). This suggests that changes in chromatin accessibility, both increases and decreases, depend on classical light signaling pathways.

For second-generation sequencing, regions such as 5S rRNA and *CEN180* are challenging to resolve. However, due to its long-read nature, Fiber-seq, a third-generation sequencing technology, can directly span repetitive regions, detecting chromatin and methylation changes in these areas (Fig. 4*D*). Unexpectedly, we found that the chromatin accessibility of the 5S rRNA and *CEN180* regions changed during photomorphogenesis. Their accessibility briefly increased at 6 h of light exposure, but generally decreased with increasing light duration (Fig. 4*E*). These patterns were also evident at the single-molecule level: in both regions, chromatin appeared more accessible in the D group than in the L group, with denser distributions of m6A signals and slightly lower mCG levels (Fig. 4*F* and *SI Appendix*, Fig. S11).

These results suggest that changes in chromatin accessibility are dependent on the integrity of light signaling pathways. The absence of light signaling pathways interferes with chromatin remodeling and may even affect the plant's adaptive regulation to its light environment.

Application of Fiber-Seq in Maize to Explore Potential Long-Range Interactions. Given maize's complex genome structure and its importance in agriculture, this study applied Fiber-seq technology to analyze its chromatin accessibility, nucleosome positioning, and mCG distribution. We performed Fiber-seq on two biological replicates of 7-d-old maize (B73). The results showed an average fragment length of 21,342 bp for the first replicate, with good data quality and high reproducibility between the two replicates (Fig. 5*A* and Dataset S1 and *SI Appendix*, Fig. S12 *A* and *C*). We performed ATAC-seq and found a modest overlap between ATAC-seq peaks and Fiber-seq peaks, with the overlap accounting for approximately 35.8% of the peaks detected by Fiber-seq. A larger portion of peaks were uniquely detected by Fiber-seq (Fig. 5*B* and Dataset S9). This may be because Fiber-seq can detect some peaks in maize genomic regions where second-generation sequencing cannot be effectively aligned, whereas ATAC-seq fails to do so (*SI Appendix*, Fig. S13). In addition, the specificity of each technique may also result in peaks detected by one method being difficult to detect with the other (*SI Appendix*, Fig. S14 *A*–*C*). Meta gene analysis revealed that ATAC-seq and FIRE signals were very similar at TSS, consistent with the heatmap results (Fig. 5*C* and *SI Appendix*, Fig. S14*D*).

To further investigate the genomic distribution of regions detected by ATAC-seq and Fiber-seq, we found that ATAC-seq-detected regions primarily reside in genic and intergenic regions. In contrast, Fiber-seq detected regions are predominantly found in TE regions, particularly nongene-associated TEs. This indicates that Fiber-seq can detect open chromatin regions distal to genes and also suggests the regulatory potential of TEs, which is consistent with the very recently published research (48) (*SI Appendix*, Fig. S15*A*). The peak distribution plot further supports this finding, showing that peaks detected by Fiber-seq are distributed not only at TSS but also at more distal regions (*SI Appendix*, Fig. S15*B*). To further explore whether peaks uniquely detected by Fiber-seq have biological functions, we conducted additional analyses. The results indicate that Fiber-seq detected regions show more TF binding (*SI Appendix*, Fig. S15*C*). Moreover, although the number of SNPs in the midpoints of all peaks is low, we identified a significant number of associations with GWAS-related signals when overlapping these peaks with enriched loci from various phenotypic GWAS datasets, suggesting that these peaks may have potential regulatory roles in maize (*SI Appendix*, Fig. S15*D*). To more clearly illustrate the regulatory role of distal peaks identified by Fiber-seq, we used Fiber-seq to detect *KERNEL ROW NUMBER 4* (*KRN4*), a classic enhancer upstream of *UNBRANCHED3* (*UB3*) (49) (Fig. 5*D*). We also found a potential enhancer approximately 105 kb downstream of *UB3*. To further verify whether this enhancer interacts with the gene, we used chromatin interaction pattern maps by Hi-C for confirmation (50, 51). We indeed observed a loop connecting *UB3* and this site, indicating that the distal peaks detected by Fiber-seq have regulatory potential, consistent with related findings (47) (*SI Appendix*, Fig. S16).

In summary, for complex plant genomes like maize, Fiber-seq identifies additional open chromatin regions often missed by traditional methods. It also facilitates the exploration of potential long-range regulatory interactions.

Fiber-Seq Contains Genomic Information. Long-read sequencing technologies can effectively address the complexity of crop genome assembly. To explore the potential application of Fiber-seq HiFi long-read sequencing data in genome assembly, we attempted de novo assembly of the maize inbred lines B73 and Jing724 (Fig. 6*A*). After quality control, the average DNA fragment length of Jing724 was 16,953 bp for the first replicate, with high data quality and good reproducibility between the two replicates (Fig. 6*B* and Dataset S1 and *SI Appendix*, Fig. S12 *B* and *D*). Subsequently, HiFi reads from the first of the two replicates were

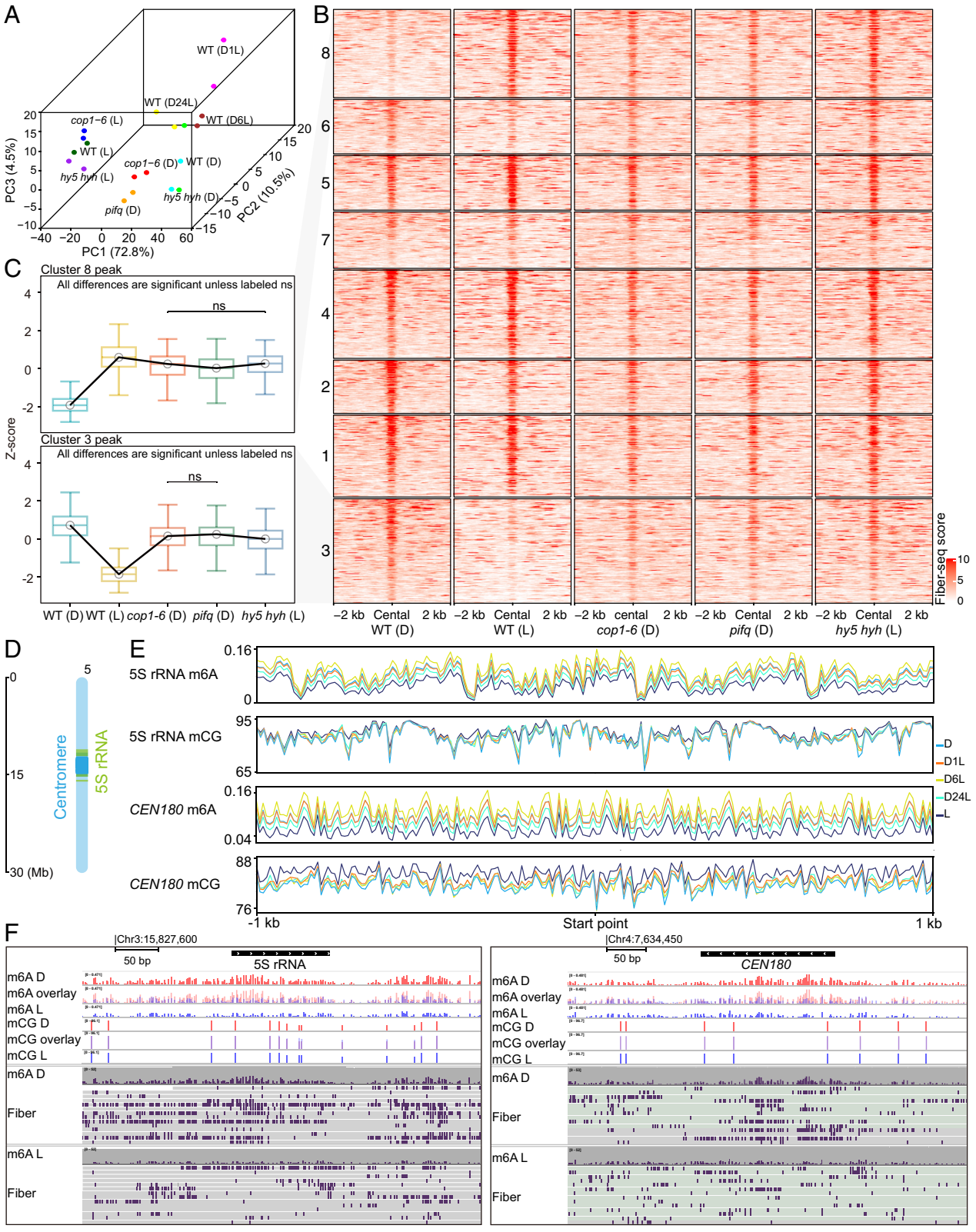

Fig. 4. Dependence of chromatin accessibility on canonical light signaling pathways. (*A*) PCA of the transcriptomes of ten samples: WT (D), WT (D1L), WT (D6L), WT (D24L), WT (L), *cop1-6* (D), *cop1-6* (L), *pifq* (D), *hy5 hyh* (D), and *hy5 hyh* (L). (*B*) Clustering of chromatin accessibility across eight clusters in WT (D), WT (L), *cop1-6* (D), *pifq* (D), and *hy5 hyh* (L). (*C*) Boxplots of accessibility for cluster 8 and cluster 3. Pairwise comparisons were performed using the Wilcoxon rank-sum test. When comparing any two groups, if the adjusted *P*-value exceeds 0.05, the difference is considered nonsignificant (ns). (*D*) Schematic diagram of centromere and 5S rRNA region distribution on chromosome 5. (*E*) Meta gene analysis of m6A and mCG levels in 5S rRNA and *CEN180* regions of *Arabidopsis* during the light transition, based on the Col-CC reference genome. (*F*) Comparison of m6A and mCG levels at individual 5S rRNA and *CEN180* loci, showing m6A, mCG, and fiber data under D and L conditions only.

used for genome assembly. Whole-genome alignments were then performed between the assembled B73 and Jing724 genomes and the B73_v5 genome, based on which structural variations (SVs, setting the minimum alignment length to 500 bp to identify SVs) were identified. On chromosome 1, 2,700 SVs were detected between our assembled B73 genome and the B73_v5 reference,

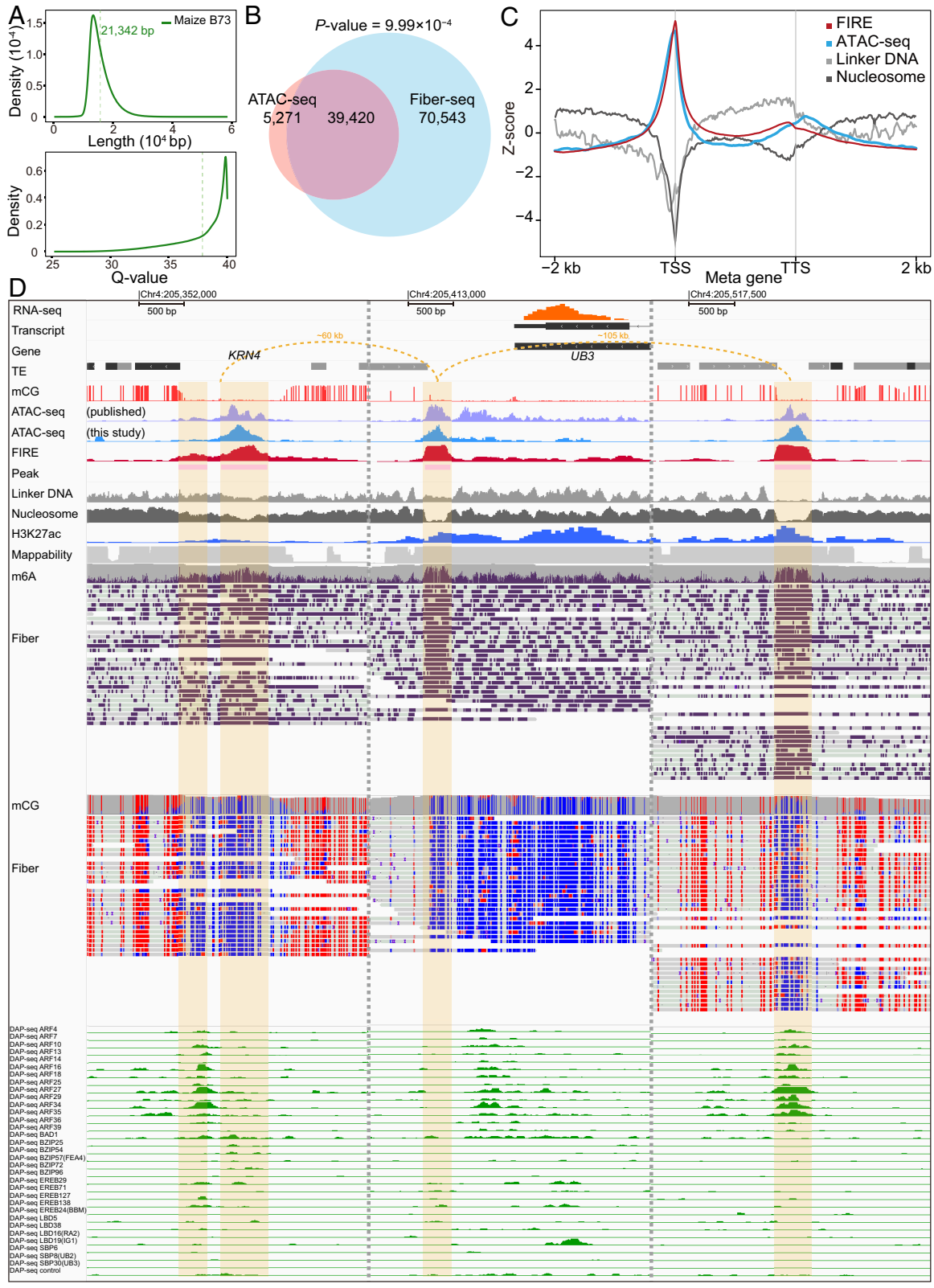

Fig. 5. Fiber-seq analysis and regulatory potential of distal open chromatin regions in maize B73. (*A*) Histogram of chromatin fiber length distribution from maize B73 Fiber-seq, showing average read length and Q-value. (*B*) Overlap of in-house-generated ATAC-seq and Fiber-seq peak counts detected in maize B73, with *P*-value calculated using a permutation test. (*C*) Meta gene analysis of FIRE, ATAC-seq peaks, linker DNA, and nucleosomes at TSS and TTS in maize B73. (*D*) Multilayered chromatin landscape at the *UNBRANCHED3 (UB3)* locus, including RNA-seq, mCG, in-house-generated ATAC-seq signal, published ATAC-seq signal (47), FIREs, peaks, linker DNA, nucleosome positions, H3K27ac, and DNA affinity purification sequencing (DAP-seq) tracks for various TFs. Additional tracks display mappability, m6A per fiber, and mCG per fiber. Chromatin fibers are shown in gray; m6A sites are marked in purple. mCG sites in red, and unmethylated regions in blue. Yellow highlights mark obvious open areas. The gray dashed lines separate three distal-distance chromatin regions. The yellow dashed lines indicate potential regulatory relationships and the distances between them.

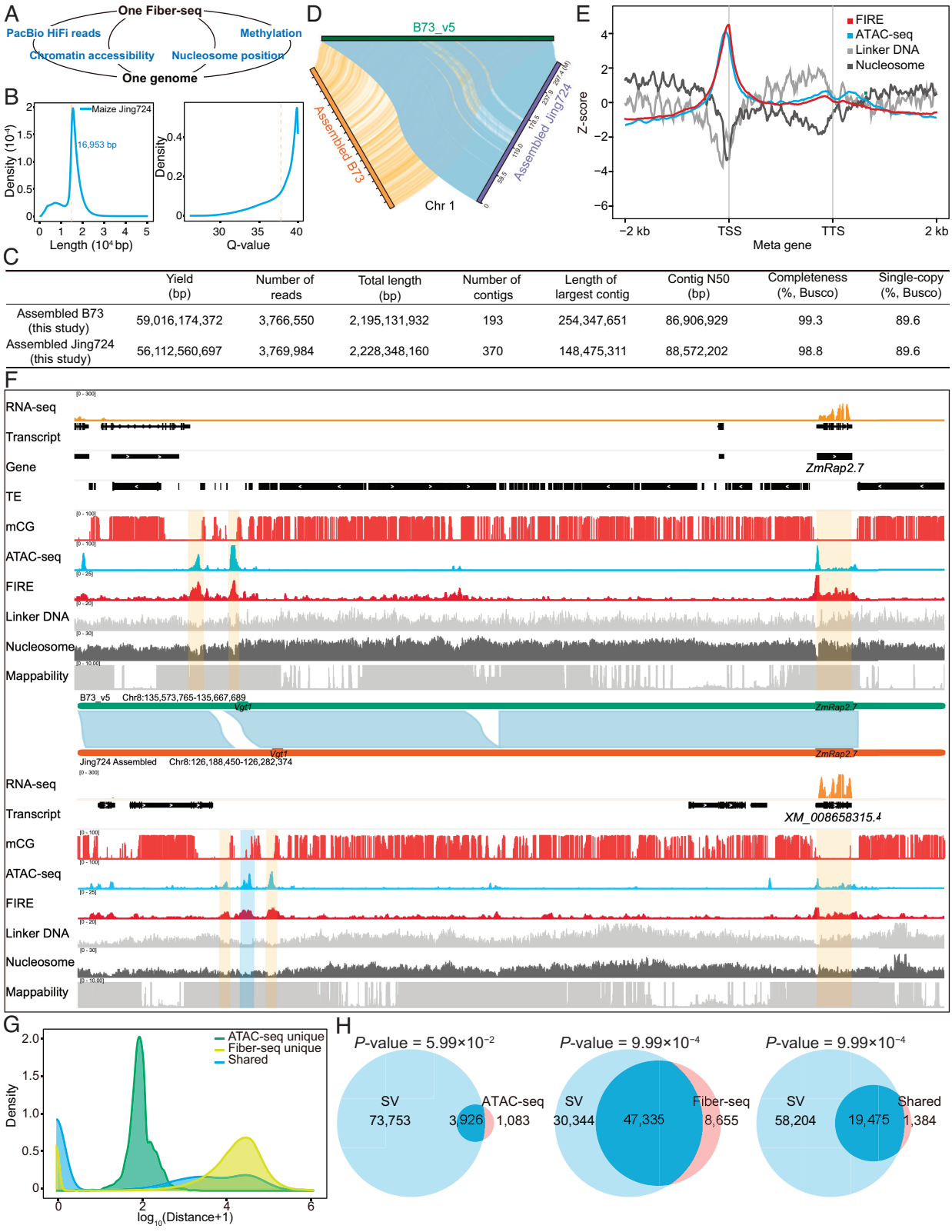

	Yield (bp)	Number of reads	Total length (bp)	Number of contigs	Length of largest contig	Contig N50 (bp)	Completeness (%, Busco)	Single-copy (%, Busco)
Assembled B73 (this study)	59,016,174,372	3,766,550	2,195,131,932	193	254,347,651	86,906,929	99.3	89.6
Assembled Jing724 (this study)	56,112,560,697	3,769,984	2,228,348,160	370	148,475,311	88,572,202	98.8	89.6

Fig. 6. Probing genome-specific chromatin states using Fiber-seq with de novo genome assembly. (*A*) A single Fiber-seq experiment yields PacBio HiFi reads along with information on chromatin accessibility, nucleosome positioning, and DNA methylation. Based on these data, a comprehensive genome and its associated epigenomic features can be obtained. (*B*) Histogram of chromatin fiber length distribution from maize Jing724 Fiber-seq, including average read length and Q-value. (*C*) Summary of assembly statistics for the B73 and Jing724 genomes generated in this study. (*D*) Alignment of the assembled B73 genome, the assembled Jing724 genome, and the B73_v5 reference genome in chromosome 1. (*E*) Meta gene analysis of FIRE, ATAC-seq peaks, linker DNA, and nucleosomes at TSS and TTS in maize Jing724. (*F*) SVs near the *RELATED TO APETALA2.7* (*ZmRap2.7*) gene and its enhancers between the Jing724 genome and the B73_v5 reference genome, along with differences in transcription and chromatin accessibility. Shown tracks include RNA-seq, mCG, ATAC-seq signal, FIRE, linker DNA, nucleosome positions, and mappability. Yellow highlights show *ZmRap2.7* and its enhancer open peaks, and accessible SV peaks are highlighted in blue. (*G*) The distances to the TSS of peaks uniquely detected by ATAC-seq, peaks uniquely detected by Fiber-seq, and peaks detected by both methods in Jing724. (*H*) Relationship between the number of SVs identified by comparing the assembled Jing74 genome with the B73_v5 genome and the number of open chromatin regions detected by ATAC-seq and Fiber-seq, as well as the number of overlapping regions between the two methods, with *P*-values calculated using permutation tests.

while 38,606 SVs were found between the assembled Jing724 genome and B73_v5 (Fig. 6 *C* and *D* and *SI Appendix*, Fig. S17). Meta gene analysis of Jing724 revealed that the distribution patterns of FIRE and ATAC-seq signals around TSS were similar. Both linker DNA and nucleosome signals were reduced near the TSS and exhibited a periodic, complementary oscillation pattern (Fig. 6*E* and *SI Appendix*, Fig. S18).

To investigate the impact of SVs on transcriptional regulation and chromatin accessibility during maize breeding, we aligned the Fiber-seq data to the de novo assembled genome of Jing724, allowing for a more accurate analysis of chromatin accessibility and structural features. Upstream of *RELATED TO APETALA2.7* (*ZmRap2.7*) lies a previously defined putative enhancer, *Vegetative to generative transition 1* (*Vgt1)* (52). We identified a SV in this region, accompanied by an accessibility peak in Jing724 compared to B73. Notably, although both *ZmRap2.7* and its enhancer region exhibited lower accessibility in Jing724 than in B73, the transcriptional level of *ZmRap2.7* was elevated (Fig. 6*F*). In Jing724, the terminator region of the *KERNEL NUMBER 6* (*KNR6*) homolog showed greater chromatin accessibility and higher gene expression compared to B73 (*SI Appendix*, Fig. S19). These findings suggest that SVs influence chromatin accessibility and gene expression, consistent with recent studies (53). We further compared the overlap between ATAC-seq and Fiber-seq signals in Jing724 and analyzed their relationship with gene features, finding a similar pattern to that observed in B73 (Fig. 6*G*). Using B73 as a reference, we investigated the relationship between SVs and chromatin accessibility in Jing724. The results revealed that SVs in Jing724 relative to B73 are often associated with chromatin accessibility. Fiber-seq enabled us to identify a large number of accessible regions overlapping with SVs; furthermore, accessible SVs uniquely detected by Fiber-seq accounted for approximately 66.9% of all open SVs (Fig. 6*H* and Dataset S10).

In summary, Fiber-seq data simultaneously enabled de novo assembly and chromatin structure analysis of maize, revealing changes in chromatin structure and gene regulation during breeding.

Discussion

In this study, we employed Fiber-seq, a technique capable of effectively distinguishing between nucleosome-occupied regions and linker DNA signals, thereby enabling comprehensive analysis of chromatin structural dynamics. During photomorphogenesis, we observed significant changes in chromatin accessibility across genes involved in light response, development, and hormone signaling, with distinct dynamic patterns among different groups. Leveraging the advantages of third-generation single-molecule sequencing, we further investigated DNA methylation levels in the 5S rRNA and centromeric regions. We conducted a preliminary study in the complex maize genome and found that Fiber-seq can identify potential distal enhancers. In conjunction with de novo genome assembly, we found that Jing724 contains a large number of accessible structural variants.

This study reveals that light influences chromatin accessibility not only at promoter regions but also at distal putative enhancer regions. These findings suggest that future investigations could leverage high-resolution chromatin conformation capture techniques, such as Micro-C-XL, to explore three-dimensional chromatin regulation and clarify the roles of distal enhancers in photomorphogenesis and gene expression. Furthermore, CRISPR-Cas9-mediated editing of individual enhancers or enhancer combinations may help validate their functional relevance in light-responsive transcriptional regulation.

A perplexing finding in our study is the relatively weak correlation between light-induced changes in chromatin accessibility and the corresponding changes in gene expression. This suggests that chromatin remodeling alone may be insufficient to predict transcriptional outcomes under light conditions directly. We have considered several possible explanations for this result. First, different cell types may possess distinct light-responsive regulatory mechanisms, but current Fiber-seq technology does not support single-cell resolution. In the future, single-cell techniques such as single-cell ATAC-seq will be better suited to capture the heterogeneity of chromatin accessibility across cell types and accurately assess the effects of light in specific cellular contexts. Second, while long-read, PCR-free methods like Fiber-seq are highly effective for mapping chromatin accessibility and detecting structural variants, the lack of signal amplification limits their utility in single-cell analyses. Alternative strategies such as deaminase-assisted single-molecule chromatin fiber sequencing (DAF-seq) and Footprinting Of Open DNA with Individual Enzymes (FOODIE), which integrate cytosine deamination–based labeling, may offer greater potential for profiling chromatin dynamics at the single-cell or ultra-low-input level (54, 55). However, these methods still face considerable technical challenges that need to be addressed before they can be widely applied in such contexts.

Another unresolved question is what determines changes in chromatin accessibility. One hypothesis suggests that it is related to the surrounding landscape of histone modifications. Additionally, chromatin remodeling factors likely play a crucial role in mediating these accessibility changes (56). For instance, the chromatin remodeling factor PICKLE (PKL) has been shown to participate in light signaling and to interact with the key photomorphogenesis regulator HY5, thereby controlling hypocotyl elongation (57). This indicates that classic light-responsive TFs may interact with chromatin remodeling factors to regulate chromatin accessibility and gene expression.

This study not only demonstrates the powerful potential of Fiber-seq technology in resolving the higher-order chromatin structure and dynamic changes of plants at near-nucleotide resolution but also reveals the profound impact of light signals on the genome at the epigenetic level. Its breakthroughs in detecting distal regulatory elements and deciphering complex genomic SVs lay a solid foundation for future research in plant precision breeding and environmental adaptation.

Materials and Methods

Plant materials and growth conditions are described in *SI Appendix*, *Materials and Methods*. The detailed procedures of m6A-MTase enzyme purification, Fiber-seq nuclei isolation, nucleic acid extraction, Fiber-seq library preparation and sequencing, ATAC-seq, RNA-seq, ATAC-seq bioinformatics analysis, RNA-seq bioinformatics analysis, Fiber-seq bioinformatics analysis, Fiber-seq score definition, genome assembly and variant screening, reference genome usage, identification of light-responsive chromatin accessibility peaks, comparative analysis of ATAC-seq and Fiber-seq peaks, SV region filtering, identification of DMRs, and differentially expressed genes are provided in *SI Appendix*, *Materials and Methods*.

Data, Materials, and Software Availability. The Fiber-seq, ATAC-seq, and RNA-seq data generated in this study have been deposited in the Genome Sequence Archive of the National Genome Data Center of China with Accession Nos.: CRA026768, CRA026769, and CRA026770 (58). SNP and GWAS data can

be obtained from maizeGDB (https://jbrowse.maizegdb.org/) (Dataset S11). All the code has been deposited in a GitHub repository (https://github.com/SunLab-NNU/Plant_Fiber) (59).

ACKNOWLEDGMENTS. We are grateful to Prof. Shuhua Xu (Fudan University) for sharing the Fiber-seq protocol. We thank Prof. Peter Quail (University of California, Berkeley) for providing *pifq*seeds. This work was supported by Shandong Provincial Natural Science Foundation (SYS202206, ZR2022ZD22, and ZR2021ZD30), the Shandong Provincial Science and Technology Innovation Fund, the National Key R&D Program of China (Grant No. 2024YFA1306701 to X.W.D.), the National Natural Science Foundation of China (Grant No. 32230006), the Priority Academic Program Development of Jiangsu Higher Education Institutions, and the "Seedling Project" of the Botanical Society of China (L.S.).

Author affiliations: [a]State Key Laboratory of Microbial Technology, College of Life Sciences, Nanjing Normal University, Nanjing 210023, China; [b]State Key Laboratory of Wheat Improvement, Peking University Institute of Advanced Agricultural Sciences, Shandong Laboratory of Advanced Agricultural Sciences at Weifang, Shandong 261000, China; [c]Peking-Tsinghua Center for Life Sciences, School of Advanced Agricultural Sciences and School of Life Sciences, Peking University, Beijing 100871, China; [d]Berry Genomics Co., Ltd., Beijing 102200, China; and [e]Vazyme Biotech Co., Ltd., Nanjing 210000, China

Author contributions: X.W.D. and L.S. designed research; L.L., G.C., G.Z., J.W., X.K., Z.Z., L.F., and L.S. performed research; M.H., W.H., Z.Q., and L.Z. contributed new reagents/analytic tools; G.C. and L.S. analyzed data; C.L., B.Z., and H.H. offered valuable guidance; and L.L., X.W.D., and L.S. wrote the paper.

1. X. Han *et al.*, Time series single-cell transcriptional atlases reveal cell fate differentiation driven by light in *Arabidopsis* seedlings. *Nat. Plants* **9**, 2095–2109 (2023).
2. Y. Jiao, O. S. Lau, X. W. Deng, Light-regulated transcriptional networks in higher plants. *Nat. Rev. Genet.* **8**, 217–230 (2007).
3. Y. Jiao, L. Ma, E. Strickland, X. W. Deng, Conservation and divergence of light-regulated genome expression patterns during seedling development in rice and *Arabidopsis*. *Plant Cell* **17**, 3239–3256 (2005).
4. L. Ma *et al.*, Light control of *Arabidopsis* development entails coordinated regulation of genome expression and cellular pathways. *Plant Cell* **13**, 2589–2607 (2001).
5. C. Yi, X. W. Deng, COP1–from plant photomorphogenesis to mammalian tumorigenesis. *Trends Cell Biol.* **15**, 618–625 (2005).
6. H. Shi *et al.*, Genome-wide regulation of light-controlled seedling morphogenesis by three families of transcription factors. *Proc. Natl. Acad. Sci. U.S.A.* **115**, 6482–6487 (2018).
7. H. Zhang *et al.*, Genome-wide mapping of the HY5-mediated gene networks in *Arabidopsis* that involve both transcriptional and post-transcriptional regulation. *Plant J.* **65**, 346–358 (2011).
8. P. Puente, N. Wei, X. W. Deng, Combinatorial interplay of promoter elements constitutes the minimal determinants for light and developmental control of gene expression in *Arabidopsis*. *EMBO J.* **15**, 3732–3743 (1996).
9. L. Guo, J. Zhou, A. A. Elling, J.-B.F. Charron, X. W. Deng, Histone modifications and expression of light-regulated genes in *Arabidopsis* are cooperatively influenced by changing light conditions. *Plant Physiol.* **147**, 2070–2083 (2008).
10. A. Nassrallah *et al.*, DET1-mediated degradation of a SAGA-like deubiquitination module controls H2Bub homeostasis. *eLife* **7**, e37892 (2018).
11. C. Bourbousse *et al.*, Histone H2B monoubiquitination facilitates the rapid modulation of gene expression during *Arabidopsis* photomorphogenesis. *PLoS Genet.* **8**, e1002825 (2012).
12. Q. Guo *et al.*, The *PIF1/PIF3-MED25-HDA19* transcriptional repression complex regulates phytochrome signaling in *Arabidopsis*. *New Phytol.* **240**, 1097–1115 (2023).
13. F. Tessadori *et al.*, Phytochrome B and histone deacetylase 6 control light-induced chromatin compaction in *Arabidopsis thaliana*. *PLoS Genet.* **5**, e1000638 (2009).
14. Z. Mao *et al.*, *Arabidopsis* cryptochrome 1 controls photomorphogenesis through regulation of H2A.Z deposition. *Plant Cell* **33**, 1961–1979 (2021).
15. Q. Cheng *et al.*, Phytochrome-interacting factor 7 and relative of early flowering 6 act in shade avoidance memory in *Arabidopsis*. *Nat. Commun.* **15**, 8032 (2024).
16. J. Kim *et al.*, Phytochrome B triggers light-dependent chromatin-remodeling through the PRC2-associated PHD finger protein, VIL1. *Nat. Plants* **7**, 1213–1219 (2021).
17. W. Wang, J. Kim, T. S. Martinez, E. Huq, S. Sung, COP1 controls light-dependent chromatin remodeling. *Proc. Natl. Acad. Sci. U.S.A.* **121**, e2312853121 (2024).
18. A. M. Sullivan *et al.*, Mapping and dynamics of regulatory DNA and transcription factor networks in A. thaliana. *Cell Rep.* **8**, 2015–2030 (2014).
19. J. Chen *et al.*, A complete telomere-to-telomere assembly of the maize genome. *Nat. Genet.* **55**, 1221–1231 (2023).
20. D. Fultz, A. McKinlay, R. Enganti, C. S. Pikaard, Sequence and epigenetic landscapes of active and silent nucleolus organizer regions in *Arabidopsis*. *Sci. Adv.* **9**, eadj4509 (2023).
21. A. M. Wenger *et al.*, Accurate circular consensus long-read sequencing improves variant detection and assembly of a human genome. *Nat. Biotechnol.* **37**, 1155–1162 (2019).
22. B. A. Flusberg *et al.*, Direct detection of DNA methylation during single-molecule, real-time sequencing. *Nat. Methods* **7**, 461–465 (2010).
23. V. Garg *et al.*, Unlocking plant genetics with telomere-to-telomere genome assemblies. *Nat. Genet.* **56**, 1788–1799 (2024).
24. A. B. Stergachis, B. M. Debo, E. Haugen, L. S. Churchman, J. A. Stamatoyannopoulos, Single-molecule regulatory architectures captured by chromatin fiber sequencing. *Science* **368**, 1449–1454 (2020).
25. A. S. Nanda *et al.*, Direct transposition of native DNA for sensitive multimodal single-molecule sequencing. *Nat. Genet.* **56**, 1300–1309 (2024).
26. W. Mo *et al.*, Single-molecule targeted accessibility and methylation sequencing of centromeres, telomeres and rDNAs in *Arabidopsis*. *Nat. Plants* **9**, 1439–1450 (2023).
27. B. Leduque, A. Edera, C. Vitte, L. Quadrana, Simultaneous profiling of chromatin accessibility and DNA methylation in complete plant genomes using long-read sequencing. *Nucleic Acids Res.* **52**, 6285–6297 (2024).
28. A. Jha *et al.*, DNA-m6A calling and integrated long-read epigenetic and genetic analysis with fibertools. *Genome Res.* **34**, 1976–1986 (2024).
29. K. C. Potter, J. Wang, G. E. Schaller, J. J. Kieber, Cytokinin modulates context-dependent chromatin accessibility through the type-B response regulators. *Nat. Plants* **4**, 1102–1111 (2018).
30. B. Zhu, W. Zhang, T. Zhang, B. Liu, J. Jiang, Genome-wide prediction and validation of intergenic enhancers in *Arabidopsis* using open chromatin signatures. *Plant Cell* **27**, 2415–2426 (2015).
31. I. R. Henderson, S. E. Jacobsen, Tandem repeats upstream of the *Arabidopsis* endogene *SDC* recruit non-CG DNA methylation and initiate siRNA spreading. *Gene Dev.* **22**, 1597–1606 (2008).
32. D. B. Lyons, D. Zilberman, DDM1 and Lsh remodelers allow methylation of DNA wrapped in nucleosomes. *eLife* **6**, e30674 (2017).
33. K. Rutowicz *et al.*, Linker histones are fine-scale chromatin architects modulating developmental decisions in *Arabidopsis*. *Genome Biol.* **20**, 157 (2019).
34. E. S. Torres, R. B. Deal, The histone variant H2A.Z and chromatin remodeler BRAHMA act coordinately and antagonistically to regulate transcription and nucleosome dynamics in *Arabidopsis*. *Plant J.* **99**, 144–162 (2019).
35. Z. Gao *et al.*, Structural and functional analyses of hub microRNAs in an integrated gene regulatory network of *Arabidopsis*. *Genomics Proteomics Bioinformatics* **20**, 747–764 (2022).
36. W. Zhang, T. Zhang, Y. Wu, J. Jiang, Genome-wide identification of regulatory DNA elements and protein-binding footprints using signatures of open chromatin in *Arabidopsis*. *Plant Cell* **24**, 2719–2731 (2012).
37. Y. Zhang *et al.*, Histone H2A monoubiquitination marks are targeted to specific sites by cohesin subunits in *Arabidopsis*. *Nat. Commun.* **14**, 1209 (2023).
38. L. Sun *et al.*, Heat stress-induced transposon activation correlates with 3d chromatin organization rearrangement in *Arabidopsis*. *Nat. Commun.* **11**, 1886 (2020).
39. L. Sun *et al.*, Mapping nucleosome-resolution chromatin organization and enhancer-promoter loops in plants using Micro-C-XL. *Nat. Commun.* **15**, 35 (2024).
40. Y. Jing, R. Lin, Transcriptional regulatory network of the light signaling pathways. *New Phytol.* **227**, 683–697 (2020).
41. P. D. Duek, C. Fankhauser, HFR1, a putative bHLH transcription factor, mediates both phytochrome A and cryptochrome signalling. *Plant J.* **34**, 827–836 (2003).
42. M. Pietrzykowska *et al.*, The light-harvesting chlorophyll a/b binding proteins Lhcb1 and Lhcb2 play complementary roles during state transitions in *Arabidopsis*. *Plant Cell* **26**, 3646–3660 (2014).
43. S. Inada, M. Ohgishi, T. Mayama, K. Okada, T. Sakai, RPT2 is a signal transducer involved in phototropic response and stomatal opening by association with phototropin 1 in *Arabidopsis* thaliana. *Plant Cell* **16**, 887–896 (2004).
44. C. Sorin, M. Salla-Martret, J. Bou-Torrent, I. Roig-Villanova, J. F. Martínez-García, ATHB4, a regulator of shade avoidance, modulates hormone response in *Arabidopsis* seedlings. *Plant J.* **59**, 266–277 (2009).
45. O. Ahrazem *et al.*, Multi-species transcriptome analyses for the regulation of crocins biosynthesis in *Crocus*. *BMC Genomics* **20**, 320 (2019).
46. S. Jansson, A guide to the *Lhc* genes and their relatives in *Arabidopsis*. *Trends Plant Sci.* **4**, 236–240 (1999).
47. W. A. Ricci *et al.*, Widespread long-range *cis*-regulatory elements in the maize genome. *Nat. Plants* **5**, 1237–1249 (2019).
48. K. L. Bubb *et al.*, The regulatory potential of transposable elements in maize. *Nat. Plants* **11**, 1181–1192 (2025).
49. Y. Du *et al.*, Unbranched3 expression and inflorescence development is mediated by Unbranched2 and the distal enhancer, KRN4, in maize. *PLoS Genet.* **16**, e1008764 (2020).
50. Y. Sun *et al.*, 3D genome architecture coordinates trans and cis-regulation of differentially expressed ear and tassel genes in maize. *Genome Biol.* **21**, 143 (2020).
51. P. Dong *et al.*, 3D chromatin architecture of large plant genomes determined by local A/B compartments. *Mol. Plant* **10**, 1497–1509 (2017).
52. P. A. Crisp *et al.*, Stable unmethylated DNA demarcates expressed genes and their *cis*-regulatory space in plant genomes. *Proc. Natl. Acad. Sci. U.S.A.* **117**, 23991–24000 (2020).
53. M. Galli *et al.*, Transcription factor binding divergence drives transcriptional and phenotypic variation in maize. *Nat. Plants* **11**, 1205–1219 (2025).
54. R. He *et al.*, Genome-wide single-cell and single-molecule footprinting of transcription factors with deaminase. *Proc. Natl. Acad. Sci. U.S.A.* **121**, e2423270121 (2024).
55. E. G. Swanson *et al.*, Deaminase-assisted single-molecule and single-cell chromatin fiber sequencing. (2024), http://biorxiv.org/lookup/doi/10.1101/2024.11.06.622310.
56. T. Yang *et al.*, Chromatin remodeling complexes regulate genome architecture in *Arabidopsis*. *Plant Cell* **34**, 2638–2651 (2022).
57. Y. Jing *et al.*, *Arabidopsis* chromatin remodeling factor PICKLE interacts with transcription factor HY5 to regulate hypocotyl cell elongation. *Plant Cell* **25**, 242–256 (2013).
58. L. Li *et al.*, Data from "Single-molecule views of chromatin accessibility and structure during photomorphogenesis". China National Center for Bioinformation. https://ngdc.cncb.ac.cn/gsub/submit/bioproject/list/PRJCA038802. Deposited 13 June 2025.
59. L. Li *et al.*, Data from "Single-molecule views of chromatin accessibility and structure during photomorphogenesis". GitHub. https://github.com/SunLab-NNU/Plant_Fiber. Deposited 17 October 2025.